A TRIDENT SCHOLAR
PROJECT REPORT

NO. 454

On the Effects of Unsteady Flow Conditions
on the Performance of a Cross Flow Hydrokinetic Turbine

by

Midshipman 1/C Benjamin H. Bailin, USN

UNITED STATES NAVAL ACADEMY
ANNAPOLIS, MARYLAND

REPORT DOCUMENTATION PAGE

Form Approved
OMB No. 0704-0188

1. REPORT DATE *(DD-MM-YYYY)* 05-22-17	2. REPORT TYPE	3. DATES COVERED *(From - To)*

4. TITLE AND SUBTITLE
On the Effects of Unsteady Flow Conditions on the Performance of a Cross Flow Hydrokinetic Turbine

5a. CONTRACT NUMBER

5b. GRANT NUMBER

5c. PROGRAM ELEMENT NUMBER

6. AUTHOR(S)
Bailin, Benjamin H.

5d. PROJECT NUMBER

5e. TASK NUMBER

5f. WORK UNIT NUMBER

7. PERFORMING ORGANIZATION NAME(S) AND ADDRESS(ES)

8. PERFORMING ORGANIZATION REPORT NUMBER

9. SPONSORING / MONITORING AGENCY NAME(S) AND ADDRESS(ES)
U.S. Naval Academy
Annapolis, MD 21402

10. SPONSOR/MONITOR'S ACRONYM(S)

11. SPONSOR/MONITOR'S REPORT NUMBER(S)
Trident Scholar Report no. 454 (2017)

12. DISTRIBUTION / AVAILABILITY STATEMENT

This document has been approved for public release; its distribution is UNLIMITED.

13. SUPPLEMENTARY NOTES

14. ABSTRACT

Hydrokinetic turbines convert the energy of flowing water into usable electricity. Axial flow and cross flow turbines are the most common forms of hydrokinetic turbine, however cross flow turbine performance and the impact of surface waves are not well understood. Tests were conducted to observe the effects of waves on the performance characteristics of a cross flow turbine promulgated by the Department of Energy's Reference Model Project, specifically Reference Model 2.

Testing of a 1:6 scale model was conducted in the large towing tank in the USNA Hydromechanics Laboratory. Baseline (no wave) turbine performance was compared to published data on the same model turbine. Additionally, tests were conducted with incident waves and at various turbine depths and various tow speeds.

The average turbine performance characteristics improved slightly as depth decreased due to acceleration of the constricted flow near the surface. Waves did not significantly change the performance of the turbine when averaged over of an entire cycle and several wave periods. This was the case even though the test waves created a velocity shear across the entire span of the blade. The waves were found to impart cyclic signatures in the torque measurement which may have consequences for instantaneous blade loading and power output from the device. A computational model was developed to predict turbine performance and compares favorably to the experiment.

15. SUBJECT TERMS
Cross flow hydrokinetic turbine, H-Darrieus, Surface gravity waves, Unsteady inflow conditions, Reference Model 2, Turbine performance

16. SECURITY CLASSIFICATION OF:			17. LIMITATION OF ABSTRACT	18. NUMBER OF PAGES	19a. NAME OF RESPONSIBLE PERSON
a. REPORT	b. ABSTRACT	c. THIS PAGE		31	19b. TELEPHONE NUMBER *(include area code)*

Standard Form 298 (Rev. 8-98)
Prescribed by ANSI Std. Z39.18

ON THE EFFECTS OF UNSTEADY FLOW CONDITIONS ON THE PERFORMANCE OF A CROSS FLOW HYDROKINETIC TURBINE

by

Midshipman 1/C Benjamin H. Bailin
United States Naval Academy
Annapolis, Maryland

_____
(signature)

Certification of Adviser(s) Approval

LCDR Ethan E. Lust, USN
Mechanical Engineering Department

_____
(signature)
_____
(date)

Professor Karen A. Flack
Mechanical Engineering Department

_____
(signature)
_____
(date)

Acceptance for the Trident Scholar Committee

Professor Maria J. Schroeder
Associate Director of Midshipman Research

_____
(signature)
_____
(date)

Abstract

Hydrokinetic turbines convert the energy of flowing water into usable electricity. Axial flow and cross flow turbines are the most common forms of hydrokinetic turbine, however cross flow turbine performance and the impact of surface waves are not well understood. Tests were conducted to observe the effects of waves on the performance characteristics of a cross flow turbine promulgated by the Department of Energy's Reference Model Project, specifically Reference Model 2.

Testing of a 1:6 scale model was conducted in the large towing tank in the Hydromechanics Laboratory. The scale model turbine had a 1.075 m diameter and blades with a height of 0.807 m and a NACA 0021 cross section. Baseline (no wave) turbine performance was compared to published data on the same model turbine. Additionally, tests were conducted with incident waves, which were scaled to be large enough to create a shear in velocity across the span of the turbine. Tests were also conducted at various turbine depths and various tow speeds which resulted in a range of Reynolds numbers.

The average turbine performance characteristics improved slightly as depth decreased due to acceleration of the constricted flow near the surface. Waves did not significantly change the performance of the turbine when averaged over of an entire cycle and several wave periods. This was the case even though the test waves created a velocity shear across the entire span of the blade. The waves were found to impart cyclic signatures in the torque measurement which may have consequences for instantaneous blade loading and power output from the device.

A computational model was developed to predict turbine performance and compares favorably to the experiment at peak turbine performance. However, the model does not accurately predict the correct power at off peak conditions.

Keywords

"Cross flow hydrokinetic turbine"
"H-Darrieus"
"Surface gravity waves"
"Unsteady inflow conditions"
"Reference Model 2"
"Turbine performance"

Acknowledgements

Table of Contents

Introduction

Increased focus on viable renewable and alternative energy sources has accompanied a growing concern with global climate change due to greenhouse gas emissions [1]. Various methods for harvesting the myriad sources of sustainable energy have been explored. One such method is the harvesting of water flow energy, or hydrokinetic energy, in oceans and rivers alike through the use of hydrokinetic turbines. There exists a large amount of untapped energy associated with tidal and riverine environments and hydrokinetic energy conversion provides an avenue to turn this energy into usable electricity. Hydrokinetic conversion via turbines could help offset some of the 4,000 terawatt-hours of electricity that the US consumes per year [2]. Specifically, the hydrokinetic resource potential in the marine environment is 1,000 terawatt-hours of energy per year [3]. In addition, hydrokinetic energy in the form of tides and currents (ocean or river) is far more predictable than wind and solar energy, which are affected by various factors such as clouds and weather systems.

Current research on the performance characteristics of cross flow hydrokinetic turbines is limited. As such, the results of this Trident project will further the understanding of the performance of cross flow hydrokinetic turbines in the presence of surface waves. Similar research has been conducted on axial flow turbines, however, cross flow turbines are less well understood and offer certain advantages that make them attractive. The most notable advantage is a simple design and implementation, including the ability to have all power generation components and instrumentation out of the water [4]. In addition, a cross flow turbine is omnidirectional with respect to current direction, has low acoustic signature, turns slowly enough that it is unlikely to harm ocean fauna, and can easily support augmentation equipment such as performance-improving ducts [5].

The goal of this research is to better understand the effects of surface waves on cross flow turbines, specifically the impact of wave motion on the amount and quality of power they produce. In order to accomplish this, experiments were conducted to measure turbine power production as a function of rotation speed relative to the current speed for no wave and wave cases. In addition, performance was modeled computationally for the two cases in order to then compare experimental results to model predictions [6].

The U.S. Navy has also demonstrated an increased focus on the use of alternative and renewable energy sources to make for a more efficient and effective fighting force. In 2009, the Secretary of the Navy issued five energy goals to transform the Department of the Navy's energy use, three of which hydrokinetic energy conversion can help the Navy achieve. First, by 2020, 50% of total energy consumption in the Navy will come from alternative sources. Second, by 2020, the Navy will use alternative sources to produce at least half of shore-based energy requirements. This is particularly important for the future of hydrokinetic turbines because they could contribute significantly to the production of shore-based power that the Navy requires. Third, the Navy will reduce petroleum use in the fleet by 50% [7]. The research and development of hydrokinetic energy convertors would help the Navy achieve its stated energy goals by providing a renewable resource easily accessible to many naval bases and installations.

Currently, hydrokinetic energy is principally extracted using large hydroelectric dams. The disadvantage of this approach is the considerable capital cost of construction and installation and the significant impact on the surrounding environment. Hydrokinetic converters differ in that they do not need to significantly alter the flow of current in order to take advantage of its energy, although they also do not produce as much power [5]. Despite lessened power production, hydrokinetic energy conversion via turbines has become a promising method of harnessing an otherwise untapped resource into usable electricity due to comparatively low cost and simple implementation.

These turbines operate in a manner similar to wind turbines; however, for two turbines of equal size, a marine turbine can produce the same power as a wind turbine with a much slower flow velocity [5] because the density of water is approximately 800 times higher than the density of air and power is proportional to the density of the flowing medium.

Hydrokinetic turbines types are most commonly classified as being either axial flow or cross flow depending on the general direction of the incoming flow relative to the orientation of the turbine output shaft. Axial and cross flow turbines are illustrated in Figure 1. These two types of turbines are at the forefront of hydrokinetic energy conversion advancement.
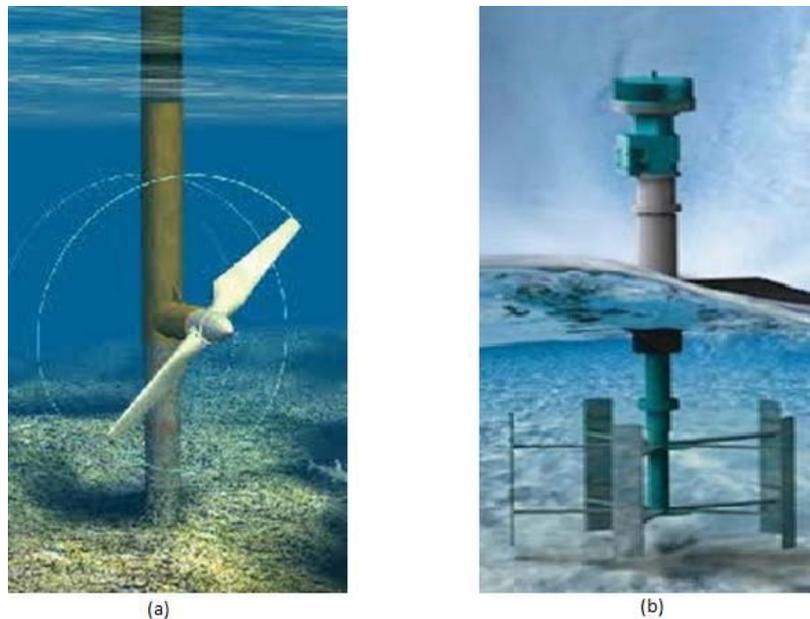

Figure 1: (a) Axial flow turbine [8]. (b) Cross flow turbine [9].

Currently, commercial systems are mostly small scale axial flow turbines, with less technology being developed for river applications than tidal applications because there is less hydrokinetic resource availability [5]. In the case of cross flow hydrokinetic turbines, limited research currently exists. Figure 2 depicts a flow chart of the classification of hydrokinetic turbines.
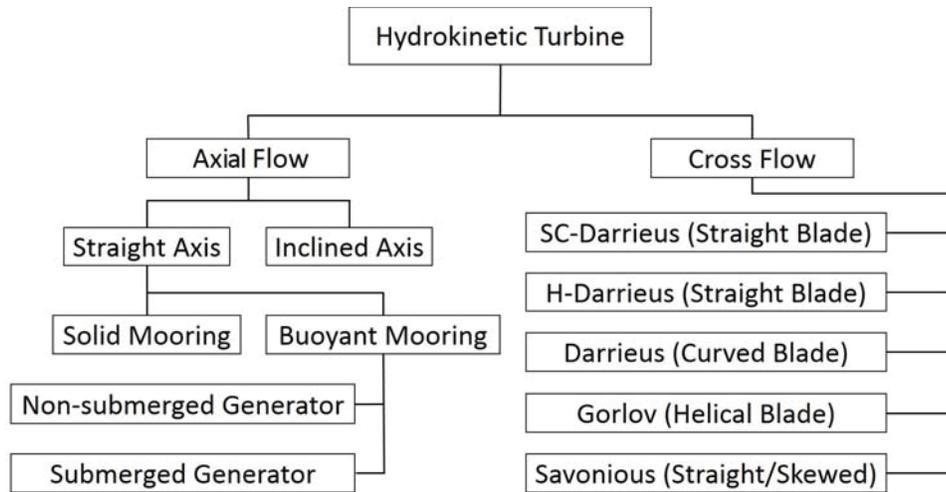
Figure 2: Classification of hydrokinetic turbines [5].

The most prominent of the cross flow turbines are Darrieus turbines, specifically the H-Darrieus and SC-Darrieus due to their simple blade design. Cross flow turbines featuring curved blades such as the parabolic shaped Darrieus, Gorlov, and Savonius turbines have not been extensively studied due to their difficulty to implement [5]. Figure 3 illustrates the shapes of the various cross flow turbines.
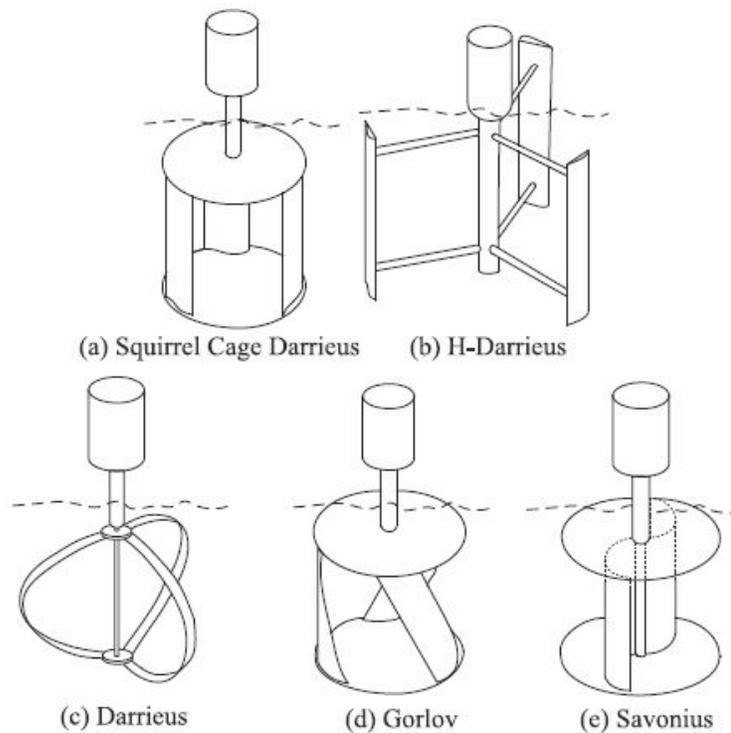

Figure 3: Common cross flow turbine designs [5].

In an effort to better understand and encourage research on hydrokinetic turbines, the Department of Energy's (DOE) Wind and Water Power Technologies Office (WWPTO) created the Reference Model Project to align with the DOE Program objective to advance the state of marine hydrokinetic (MHK) technology. The Reference Model Project created three hydrokinetic convertor reference models and three wave energy convertor reference models to act as benchmarks for further study. These benchmarks will allow for a deeper understanding of performance and costs of hydrokinetic turbines, as well as identify important technical obstacles and cost drivers that require more study [3].

One of these reference models, Reference Model 2 (RM2) is a dual rotor cross flow hydrokinetic turbine designed for use in a riverine environment, specifically in the lower Mississippi River near Baton Rouge, Louisiana (Figure 4) [10]. RM2 floats on the surface of the river through the use of two 20 m long pontoons that are cable-moored and connected with three 19 m long cross bridges. The frame that holds the two cross flow rotors extends 9.48 m into the water from the top of the pontoons. This design takes advantage of the ability for cross flow turbines to keep electrical equipment above the water and dry. Each rotor is 6.5 m in diameter and rotates opposite the other [8, 9].
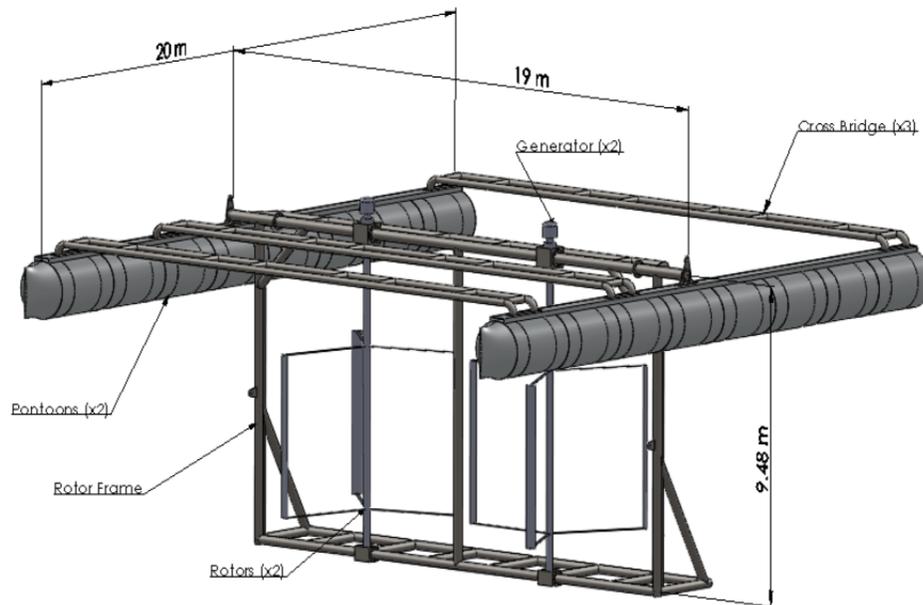

Figure 4: Reference Model 2 dual rotor cross flow turbine developed by the WWPTO [11].

The recoverable riverine hydrokinetic resource in the continental United States alone can contribute up to 120 TWh per year of energy to the U.S. power demand [12]. In addition, working in open-ocean marine environments is more difficult and more costly than working in riverine environments [13]. The disadvantage of working in rivers, however, is that they can have wide variations in flow and depth and can require many years to obtain meaningful statistics describing their flow [12]. The associated flow variation in rivers creates the necessity to study the performance of RM2 under surface waves in order to provide a better understanding of how it will operate in unsteady flow conditions.

Methods of Analysis

Hydrokinetic turbines act as energy convertors by turning kinetic energy of water flow into electricity using an electric generator. The turbine is held in a fixed position relative to the flow. In the case of RM2, the turbine is held fixed near the surface of the water by cable-moored pontoons. The river water flows over the turbine blades and generates lift to turn the turbine. The turning turbine creates a torque on a shaft connected to an electric generator, which converts the rotating motion of the shaft into electricity.

Over the span of a single rotation, lift and drag forces continuously change on each turbine blade based on its angular position. Figure 5 depicts the changing lift and drag forces with respect to a constant relative incident flow velocity. The turbine radius is denoted as R and α is the angle of attack of the turbine blade with respect to the relative velocity, the resultant of the incident flow U_∞ and turbine rotation Rω, where ω is the turbine rotational speed. At the positions in which the turbine blades act parallel to the incident flow velocity (0° and 180° positions) the torque is significantly lower and can be negative. This occurs due to the only resultant force being the drag force that opposes the direction of rotation. At the positions in which the turbine blades act perpendicular to the incident flow (90° and 270° positions) the resultant lift force is higher than the resultant drag force and the torque is therefore positive. With proper airfoil design, the total average torque per revolution of the turbine will be positive allowing for continuous rotation and electrical generation.
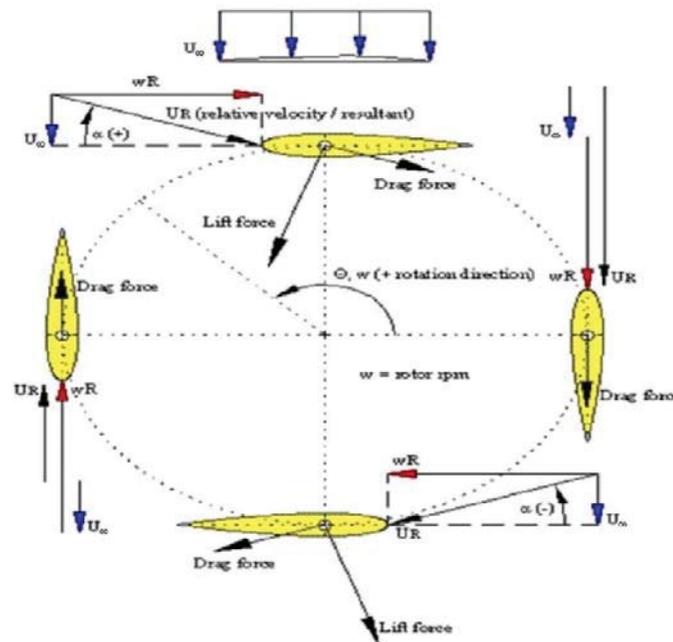

Figure 5: Lift and drag forces on a rotating cross flow turbine with blade speeds greater than or equal to three times the incident flow velocity [14].

Figure 6 illustrates the lift force, L, and drag force, D, as well as their resultant components, F_n (normal) and F_t (tangential) on a single airfoil based on a specific incident relative flow velocity,

U_R. The angle of attack of the airfoil is denoted as α. The tangential force is responsible for driving the airfoil through the flow and is therefore reponsible for the rotation of the turbine.
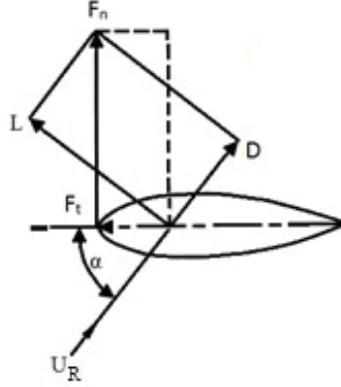

Figure 6: Single airfoil demonstrating lift and drag forces and the normal and tangential components of their resultant [15].

A computational model, implemented in MATLAB, was developed to predict turbine performance and produce results that can be compared to experimental data obtained in towing tank testing. The model is a numerical implementation of an analytical solution, solving for torque as a function of angular position. For each angular position the relative velocity and angle of attack are determined. The angle of attack is compared to empirical lift and drag data to determine the forces on the blade. The tangential and normal forces shown in Figure 6 are a function of the azimuthal position angle shown in Figure 5, θ. By integrating over all θ, the average tangential force for a single blade, $\bar{F}_t$, can be calculated:

$$\bar{F}_t = \frac{1}{2\pi} \int_0^{2\pi} F_t(\theta) \, d\theta \tag{1}$$

Using $\bar{F}_t$, the number of blades on the turbine, N, and the radius of the turbine, R, the total torque, Q, developed by the turbine on the shaft can be calculated:

$$Q = N\bar{F}_t R \tag{2}$$

The total power of the turbine, P, is then calculated using Q and the angular velocity of the turbine, ω.

$$P = Q\omega \tag{3}$$

The coefficient of power, C_P, is the ratio of the power developed by the turbine to the available power in the fluid flow [13]. The available power in the flow is calculated using the density of the fluid, ρ, the velocity of the water, U_∞, and the swept area of the turbine blades, A.

$$C_P = \frac{P}{\frac{1}{2}\rho U_\infty{}^3 A}$$

(4)

The area, A, is calculated using the radius of the turbine, R, and the height of the blade, H:

$$A = 2RH$$

(5)

The power coefficient is shown to be a function of tip speed ratio (TSR). TSR is the ratio between the tangential speed of the turbine blade (turbine radius multiplied by the rotational speed), $R\omega$, to the flow speed, U_∞:

$$TSR = \frac{R\omega}{U_\infty}$$

(6)

Figure 7 illustrates that this model calculates the forces on a single blade and then iterates for N turbine blades to arrive at the average tangential force. This model assumes uniform inflow to each blade and does not incorporate more complex hydrodynamics such as tip losses, strut losses, or the wake from upstream blades interacting with downstream blades.
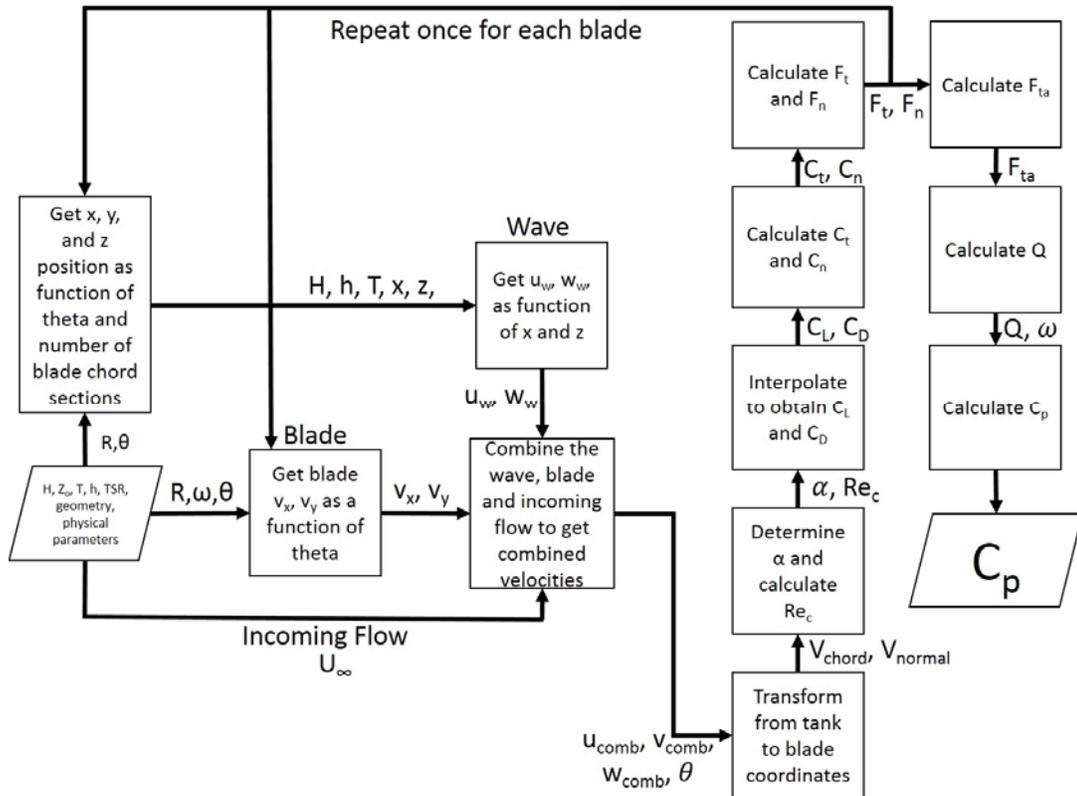

Figure 7: Modeling flowchart.

First, the position and velocity of the first blade were calculated as a function of phase angle. This velocity was combined with the incoming flow velocity and the incident wave velocity to determine the combined velocity on the blade in three dimensions.

Wave velocities are calculated as a function of the depth underneath the wave, z, time-phase of the wave, t, and phase position, x, for a finite depth utilizing the wave frequency, ω, wave amplitude, A, wave number, k, and towing tank depth, h [16]:

$$u_w = \omega \frac{H}{2} \frac{\cosh k(z+h)}{\sinh kh} \sin(\omega t - kx) \tag{7}$$

$$w_w = \omega \frac{H}{2} \frac{\sinh k(z+h)}{\sinh kh} \cos(\omega t - kx) \tag{8}$$

In order to account for both the rotation of the turbine blades in addition to the passage of the surface waves, the two parameters were related through the implementation of a time-step approach. Beginning at time zero, a small time-step moved the turbine blade around its rotation, and for each new position, the incident wave would also be stepped forward in time. This required setting the spatial phase change in the sinusoidal functions of Equations 7 and 8 to zero and only stepping the wave velocities forward in time.

Integration of the forces in the spanwise direction are also included in this model. They are utilized to calculate wave velocities at various depths and then integrated across the span of the blade to determine the overall average tangential force. Each turbine blade is split into m sections in the spanwise direction and combined velocities are calculated at the center of each section in order to account for changing wave velocities as a function of depth.

This combined velocity at each section of the blade was then transformed from tank coordinates to blade coordinates such that the chord and normal components of the velocity could be calculated with respect to the blade. These velocity components were then utilized to calculate the angle of attack and chord based Reynolds number, which could then be applied to empirical data to determine the lift and drag on the blade (Figure 8 and Figure 9, respectively).

This process was then iterated once for each blade, in this case three blades set 120 degrees apart. After the forces were calculated for each blade, they were integrated into the average tangential force on the blades (Eqn. 1). The average tangential force was then utilized to calculate the turbine torque and finally the coefficient of power.
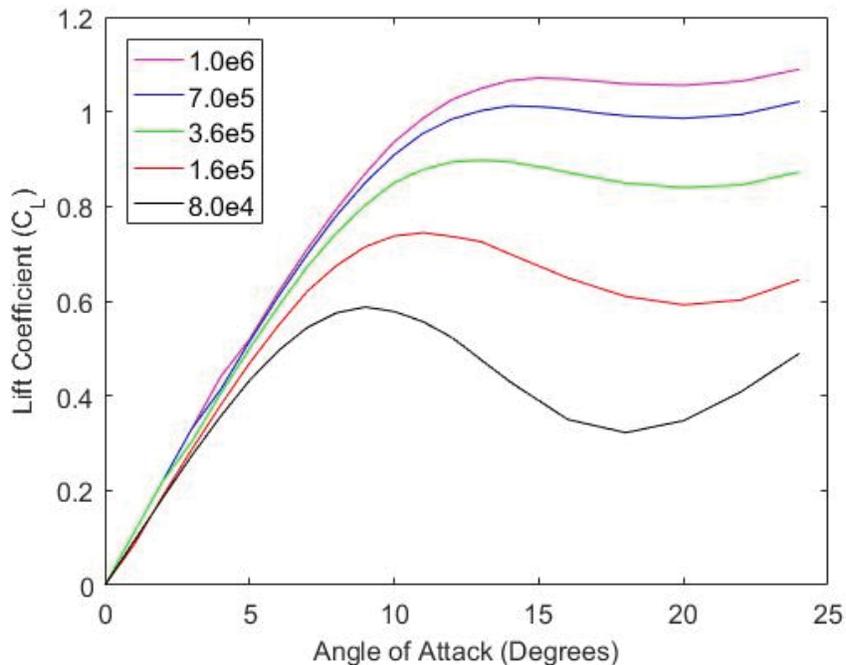
Figure 8: Experimental lift coefficient data published by Sandia National Labs for the NACA 0021 airfoil at various Reynolds numbers [17].
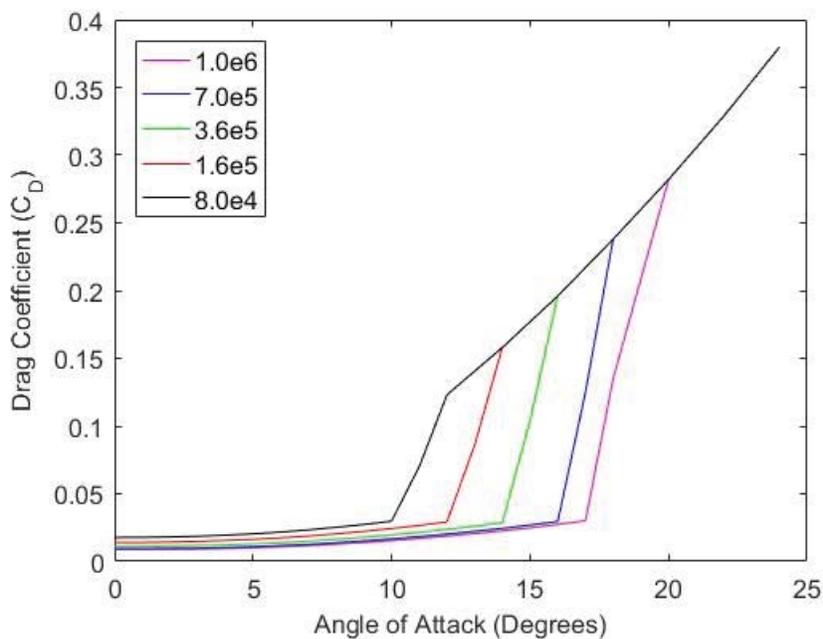

Figure 9: Experimental drag coefficient data published by Sandia National Labs for the NACA 0021 airfoil at various Reynolds numbers [17].

Experimental Details
Overview

Various experiments with the 1:6 scale model turbine were conducted in the large towing tank in the Rickover Hydromechanics Laboratory. The first set of experiments was conducted by towing the turbine model at a constant forward speed while varying turbine rotation speed in order to gather baseline results on the performance of the model turbine. Tests were also conducted at various depths, carriage speeds and wave parameters (Figure 10).
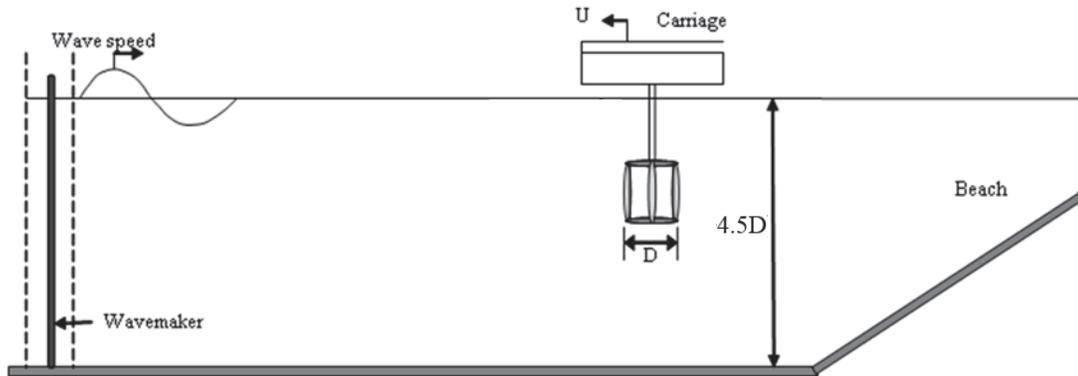

Figure 10: Sketch of towing tank experiment under unsteady flow conditions. D = 1.075 m. Tank water depth H = 4.9 m (~4.5D).

The towing tank measures 116 m long, 7.9 m wide, and 4.9 m deep. The tank features a dual-flap, servo controlled wave maker that is capable of producing waves with a maximum amplitude of 0.6 m and a frequency range of 0.25-1.25 Hz [18].

1:6 Scale Model Turbine

The turbine used in this experiment was a 1:6 scale model based on a three-bladed cross-flow design, Reference Model 2 (RM2), promulgated by the U.S. National Renewable Energy Laboratory (NREL). Table 1 illustrates the dimensions of both the full scale RM2 turbine and the 1:6 scale model turbine utilized during the experiment.

Table 1: RM2 turbine geometric parameters [19].

Parameter	Full Scale	Model (1:6)
Diameter (m)	6.450	1.075
Height (m)	4.840	0.807
Blade root chord (m)	0.400	0.067
Blade tip chord (m)	0.240	0.0400
Blade profile	NACA 0021	NACA 0021
Blade mount	½ chord	½ chord
Blade pitch (deg)	0.0	0.0
Strut profile	NACA 0021	NACA 0021
Strut chord (m)	0.3600	0.0600
Shaft diameter (m)	0.4160	0.0635

The model is 1.075 m in diameter and 0.807 m in height. The blades are symmetric with a blade pitch of 0° along the length of the blade and a NACA 0021 profile. Figure 11 shows a drawing of the model turbine as it appears attached to a 2.5 in. diameter shaft.
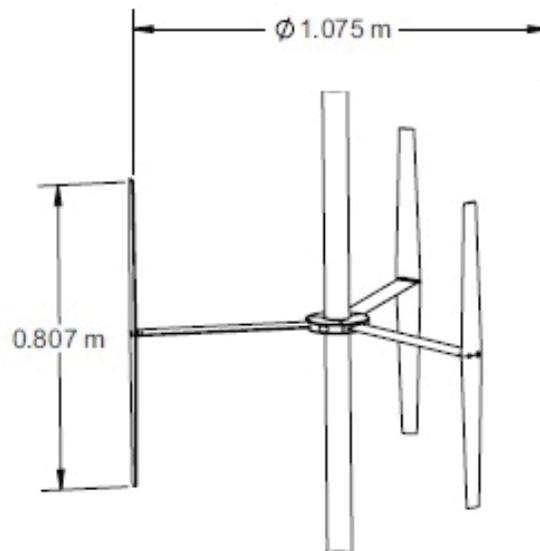

Figure 11: A drawing of the model turbine [19].

The blockage ratio is defined as the ratio of the frontal area of the turbine to the cross-sectional area of the towing tank. As the blockage ratio increases, the influence of the tank walls on the inflow velocity experienced by the turbine also increases. This artificially increases the turbine performance above what it would be in an unblocked operating environment. In a tank with a significant blockage ratio, a blockage correction must be applied to the data in order to demonstrate true turbine performance in free stream conditions [21]. The blockage ratio for the present experiment was calculated to be 2%. Blockage was therefore assumed to have a negligible effect.

Experimental Setup

All experimental and data acquisition equipment were mounted to a carriage in the large towing tank.

Table 2 summarizes the instrumentation used during this experiment, and the experimental setup is pictured in Figure 12 and Figure 13.

Table 2: Experimental instrumentation.

Measurement	Instrument
Carriage Velocity	Optical Encoder (installed in towing tank facility)
Drag	Hydronautics Inc. Block Gages
Torque	Futek Torque Sensor
Rotation Speed	BEI Sensors Incremental Optical Encoder
Reference Blade Position	BEI Sensors Incremental Optical Encoder
Wave Height	Senix Optical Sensors

Drag was measured by utilizing two block gages mounted just above each bearing housing on the test rig (Figure 12 and Figure 13). The upper block gage measured a tensile drag force and the bottom block gage measured a compressive drag force as the flow of water was modeled as a single point load on the bottom of the turbine shaft. The two block gage measurements were then summed to obtain the total drag of the turbine during each test. Due to excessive freedom of movement within the block gage mounts, drag measurements during each run had too much variability and were not analyzed.

Torque was measured using a Futek FSH01991 torque sensor with a 200 N-m limit, mounted in line with the turbine shaft (Figure 12).

Shaft rotation speed and blade position were measured using a BEI Sensors HS35 incremental optical encoder. This sensor was also mounted in line with the turbine shaft, as shown in Figure 12, and provided a high resolution measure of turbine rotational speed. The encoder counts 3,600 pulses per revolution or 10 pulses per degree providing a resolution of 0.1° [21]. Additionally, a single pulse was recorded at a fixed angular position on the drive shaft for reference.

Surface and wave elevation were measured utilizing one Senix TSPC 21S-232 optical wave height sensor placed alongside the shaft of the turbine about one diameter from the turbine centerline on the starboard side.

A Baldor BSM80N-350AF motor and controller were used to control the rotational speed of the turbine, and in turn, the tip speed ratio. The setup required additional resistors in order to allow the motor to discharge sufficient power to maintain the required rotation speeds in operating regimes at which the motor was supplying torque to oppose the motion of the turbine (i.e. braking).

For all experiments, the carriage was towed at a range of speeds between 3 and 5.5 fps. All instruments were synchronized in time, data was sampled at a rate of 1 kHz, and each run provided 20 – 60 sec of steady state data.
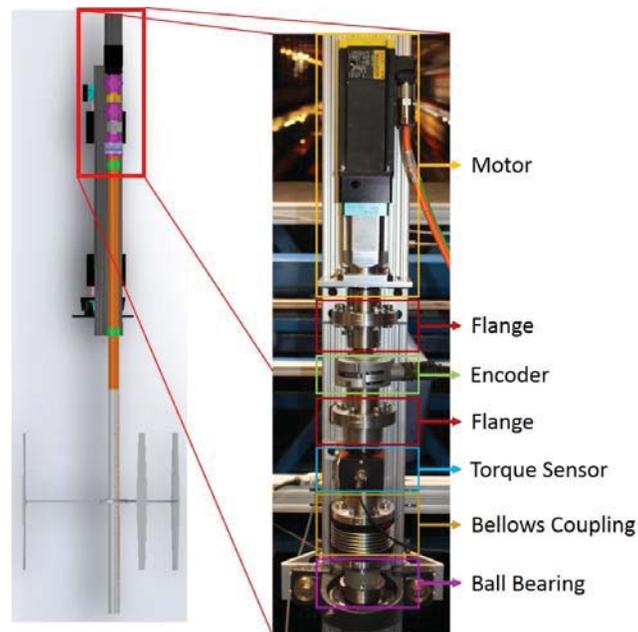

Figure 12: CAD model and close-up of top section of the experimental setup.
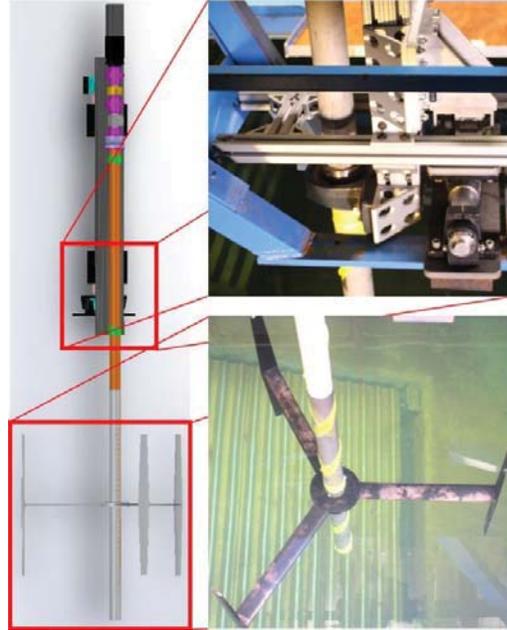
Figure 13: CAD model and close-up of bottom section of the experimental setup.

Wave Scaling

Surface gravity waves induce unsteady velocity variations in two coordinate directions. Modeled as regular waves, these periodic variations influence the flow parallel to the direction of propagation (horizontal) and perpendicular to it in the vertical direction. The extent to which the velocity varies as well as the depths of the wave influence are functions of the wave parameters such as wavelength and height, and the depth of the water column through which the waves are propagating.

Waves are generally classified by their relative depth (h/λ), which is the water depth, h normalized by the wavelength λ [22]. The experiment was designed to model unsteady flow conditions that the full scale turbine would experience based on matching the relative depth of the full scale waves to the relative depth of the model waves.

The waves selected for this experiment were intended to represent waves typically found in the lower Mississippi River and the Gulf of Mexico near the mouth of the Mississippi River where RM2 is proposed to be deployed. A literature review concluded that these waves were determined to typically be deep waveforms with periods between 3 and 6 sec [23]. A deep water waveform does not require that the water column that the wave passes over be deep, but rather that the relative depth of the wave exceed 0.5 [22].

More important than accurately modeling the waves expected to appear in the lower Mississippi River, however, was assessing the impact of unsteady velocities on turbine span of each blade. The resulting scaled model waves were therefore chosen to create a velocity shear across the entire span of each blade and the parameters are detailed in

Table 3. The relative depth of the scaled waves are classified as deep waves [22].
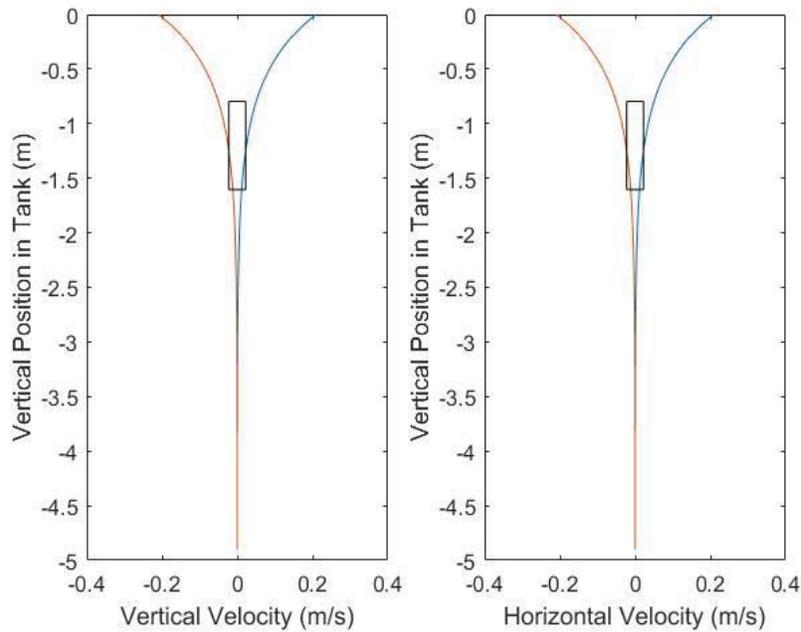
Figure 14: Velocity profile of the 0.1 m height and 1.5 sec period wave utilized during experimentation. The vertical axis is the depth below the surface of the water in the towing tank, and the horizontal axis is the vertical and horizontal velocities of the incoming waves at varying depths. The red and blue lines indicate the bounds of the wave velocity as it passes from peak to trough. The rectangle in the middle of each figure represents the area of RM2 in the water channel.
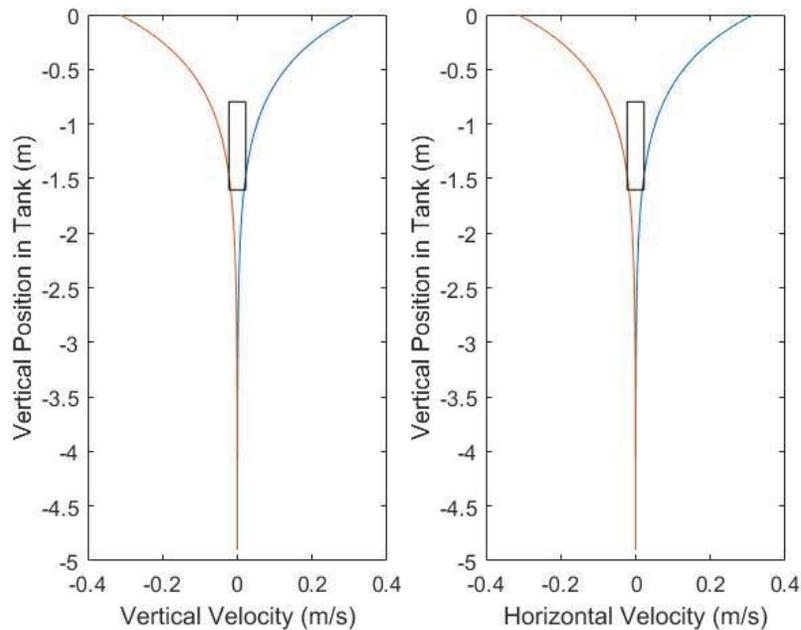

Figure 15: Velocity profile of the 0.15 m height and 1.5 sec period wave utilized during experimentation.
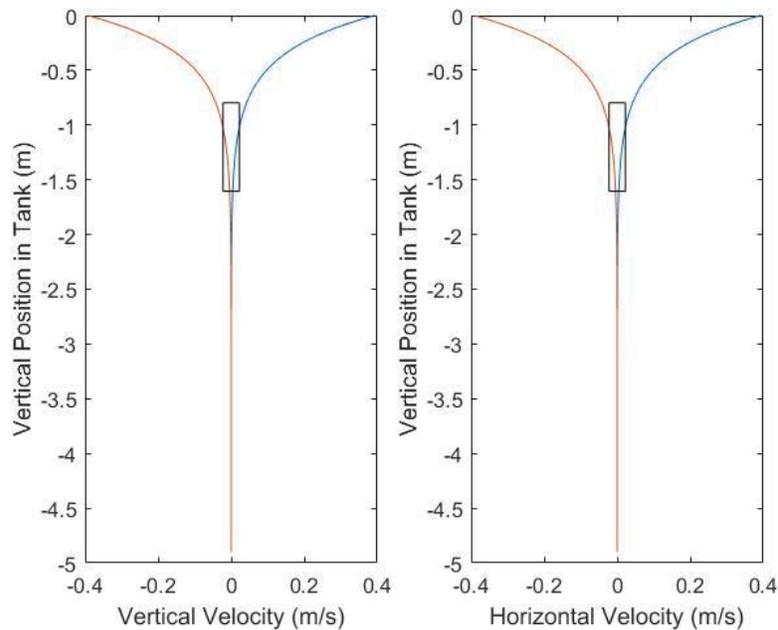
Figure 16: Velocity profile of the 0.15 m height and 1.2 sec period wave utilized during experimentation.

Figure 14, Figure 15, and Figure 16 show that at maximum velocity the shear over the span of the blades in both the vertical and horizontal directions created by the model wave is on the order of 5 cm/s, or about 5% of the incoming flow velocity.

Table 3 demonstrates the model wave parameters selected for testing.

Table 3: Model wave parameters.

Relative Depth h/λ	Wave Height, H (m)	Wavelength, λ (m)	Wave Period, T (s)	Wave Energy (J/m)
1.4	0.10	3.5	1.5	42.8
1.4	0.15	3.5	1.5	96.4
2.2	0.15	2.2	1.2	26.9

The wave energy per unit width increases proportional to the wavelength and the significant wave height squared, thus each of the three model waves have different specific energies.

Experimental Procedure

The data collection process for this experiment consisted of multiple runs (i.e. traverses of the towing tank) at varying tip speed ratios in order to assess the performance characteristics of the

turbine at various operating conditions. Several of the peak operating conditions were repeated during testing in order to verify the repeatability of the data.

Data collection from all instruments was synchronized and sampled at 1 kHz. Measurements included carriage velocity, turbine rotational speed, torque, blade position (i.e. Z-pulse), and wave height.

Prior to each run, measurements were taken for each instrument in order to "zero" out any noise and address potential sources of bias error. Turbine rotation was then initiated by an operator on the carriage and data collection was then initiated prior to carriage movement. Tests were run at carriage speeds between 3 and 5.5 fps, and data collection lasted for 60 – 90 seconds. This resulted in about 20 – 60 seconds of steady state carriage travel down the length of the towing tank. During three weeks of experiments in late January and early February, over 150 data sets were collected. Of the 150 runs conducted, 28 runs were dedicated to determining the performance characteristics under steady flow conditions and 15 runs under deep wave conditions. In addition, 8 tare tests were conducted under steady flow conditions and 7 tare tests were conducted under deep wave conditions.

Results and Discussion
Summary
From the experimental data performance characteristics of the model turbine were evaluated with and without the presence of surface waves. In addition, model performance was evaluated at various diameter-based Reynolds numbers and various tip depths (defined as the depth of the top tip of the turbine to the quiescent free surface). From the torque, rotational speed, and carriage velocity, average values for the coefficient of power (C_P) and the tip speed ratio (TSR) were calculated for each run. For all cases, C_P was plotted against TSR, illustrating the performance curves associated with the model turbine at various Reynolds numbers (Figure 17), various blade tip depths (Figure 18), no wave and wave cases (Figure 19) and the model prediction versus experimental data. (Figure 26).

The power coefficient was given by Equation 4, and tip speed ratio was given by Equation 6. In order to find the maximum power coefficient and create a range of TSR values over which the performance could be characterized, TSR was varied from 2 to 5 [19].

Performance Characteristics: Varying Reynolds Number
The coefficient of power averaged over an entire run plotted versus tip speed ratio for tests at various Reynolds numbers under steady flow conditions are shown in Figure 17. Each point on the graph corresponds to a single experimental run. The x-marks on the plot represent data gathered by Bachant and Wosnik [19] during their testing of the model turbine at the University of New Hampshire in 2014, and the closed shapes represent the testing done in January 2017 at the Naval

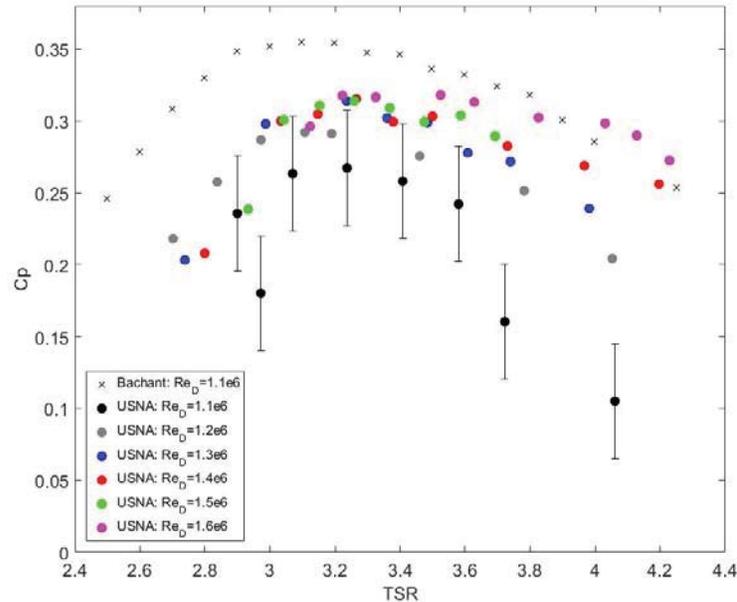Academy. The error bars plotted for a Reynolds number of 1.1×10^6 are quoted at 95% confidence.

Figure 17: Baseline performance characterization of the model turbine at various Reynolds numbers under steady conditions. The x-marks represent previous data from Bachant and Wosnik [19] and closed shapes represent the testing done in the Naval Academy's large towing tank.

The shape of the steady flow data gathered in testing at USNA compares favorably to previous data gathered by Bachant and Wosnik [19], however, their tests indicate higher performance characteristics at similar Reynolds numbers. This is likely due to the fact that in the tests conducted at UNH, blockage effects were not taken into account. Blockage effects artificially improve the performance of the turbine due to an increased incident flow velocity on the turbine caused by boundary layers along the walls of the towing tank. Blockage in the UNH towing tank was estimated to be on the order of 10%, whereas in the USNA large towing tank it was estimated to be on the order of 2%. This would indicate that turbine peak power is more accurately recorded at a TSR of 3.2 as $C_p = 0.32$ rather than $C_p = 0.35$ as previously reported.

Tip speed ratios from 2-5 were tested in order to characterize the peak of the power coefficient curve. Tip speed ratios below 2 and above 5 produce very little power. At very low TSR values, a large amount of the incoming flow of water passes through the turbine blades. Therefore, the turbine is inefficient in extracting much of the available energy in the incoming flow. As the TSR is increased, more energy is captured by the turbine blades as they spin faster and create more torque on the turbine shaft. At a TSR of approximately 3.2, however, the optimal operating point of the turbine is reached and the maximum ratio of power generated by the turbine to the available

power in the flow is achieved. At TSR values above the peak, increased turbine rotation rate causes blade drag forces to overcome lift forces and degrade power.

An important aspect of scale testing is ensuring scale independence of results. This allows scale model results to be used directly for a full scale apparatus. For the cross flow turbine, the most important parameters that need to be scale independent are the lift and drag coefficients of the foil section used in the turbine. Lift and drag coefficients are functions of Reynolds number up to a threshold and then become independent of Reynolds number. The diameter based Reynolds number used for this study is given by Equation 7:

$$Re_D = \frac{U_\infty D}{\nu} \qquad (7)$$

where U_∞ is the incident flow velocity, D is the diameter of the model turbine, and ν is the kinematic viscosity of the flowing fluid. Reynolds number independence is achieved when an increase in the model turbine's Reynolds number no longer demonstrates an increase in the associated power curve, indicating the tests reached scale independence. In order to increase the Reynolds number while still testing over the same range of tip speed ratios, both the carriage speed and rotational speed need to increase simultaneously (Eqn. 6 & 7). Due to limitations on the test rig and the large torque created by the turbine at high rotation rates, the diameter based Reynolds number was not tested beyond 1.6×10^6. These results indicate that Reynolds number independence was not reached during testing. As the Reynolds number increases and approaches a value of 1.6×10^6, the power coefficient curves begin to fall close together in value, indicating that the test was nearing Reynolds number independence, but ultimately did not achieve it.

Performance Characteristics: Varying Blade Tip Depth

Turbine performance as a function of blade tip depth was also tested. The results are shown in Figure 18 for three tip depths. Turbine performance increased as tip depth was decreased from 0.75 m to 0.38 m. Performance, however, was not drastically affected for depths less than 0.38 m. It is hypothesized that as the tip depth decreased from 0.75 m to 0.38 m, the free surface of the flow acted as a boundary, constricting the flow area near the surface which increases the flow velocity. The increased flow speed near the surface may be the reason for the modest improvement in power coefficient. As depth was decreased further from 0.38 m to 0.20 m, the turbine and free surface may have acted more like an obstruction, reducing the local flow speed and decreasing performance. These results indicate that it is beneficial to place a turbine near the free surface up

to approximately half a blade height from the surface, a positive result for floating turbine systems similar to RM2.
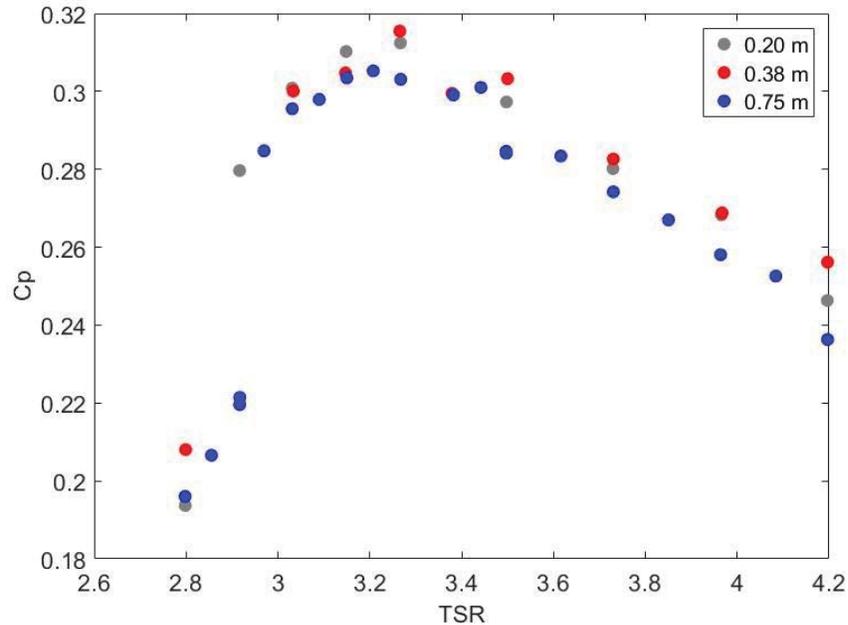

Figure 18: Performance characterization of the model turbine under steady flow conditions at various blade tip depths. All tests were conducted at a diameter based Reynolds number of 1.4×10^6.

Performance Characteristics: Unsteady Flow Conditions

The effects of unsteady flow conditions due to waves on the average coefficient of power of the model turbine is compared to steady flow conditions in Figure 19. Also shown are uncertainty bars for the no wave case, as discussed further in Appendix A. Tests were conducted at a diameter based Reynolds number of 1.4×10^6 due to the high thrust created at faster tow speeds. On average, the tests conducted under wave conditions exhibit a minimal effect on the average performance of the turbine. The peak power generated by the turbine under unsteady conditions is approximately 3% lower than the peak power produced by the turbine under steady conditions. This is well within the uncertainty of the experimental measurements.

For an entire wave phase, unsteady flow velocities generated by incident surface waves negatively impacts the performance of one or more turbine blades while positively impacting others. The unsteady velocity caused by the wave changes the incident flow velocity over the turbine blades, and therefore changes the angle of attack and lift that that blade would otherwise

generate. On average, the combination of improving one blade's performance while degrading another's causes the turbine to perform similarly as to when there are no waves present at all.
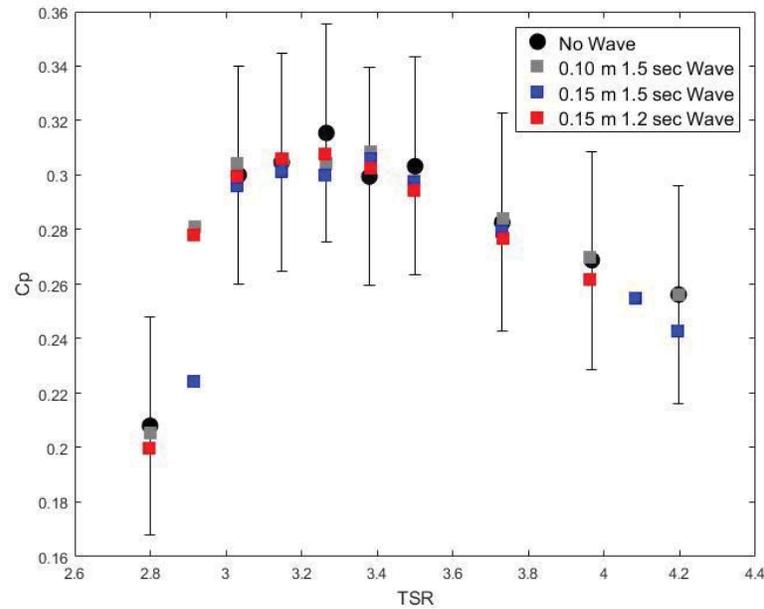

Figure 19: Performance characterization of the model turbine under steady and unsteady wave conditions. The black circles represent the no wave case. The colored squares represent wave cases at various wave parameters. All tests were conducted at a diameter based Reynolds number of 1.4×10^6.

The instantaneous performance, however, is affected by the presence of waves. Figure 20 shows the turbine torque under steady conditions and Figure 21 shows the turbine torque under unsteady (wave) conditions. Superimposed on Figure 21 is the incident wave height. Each peak and trough represents the superposition of the generated torque on all three blades. There is a fairly consistent maximum and minimum torque signal for the 5 sec of data collection shown on the plot for the steady case with variations on the order of 3-5 ft-lbs. Figure 21 illustrates that the torque produced by the turbine varies with wave phase due to the unsteady velocity associated with the incoming waves. The wave phase is evident in the cyclic nature of the torque peaks in Figure 21. This indicates that the blades likely experience variable loading and produce varying power quality when exposed to unsteady velocities. The wave influence is less significant than for axial flow turbine since the blades are generating lift in a range of the wave phase [18].
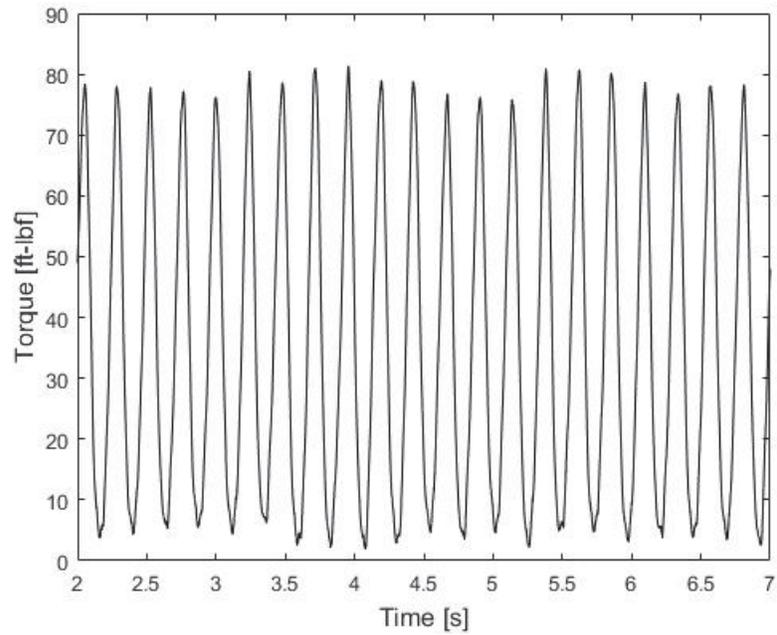
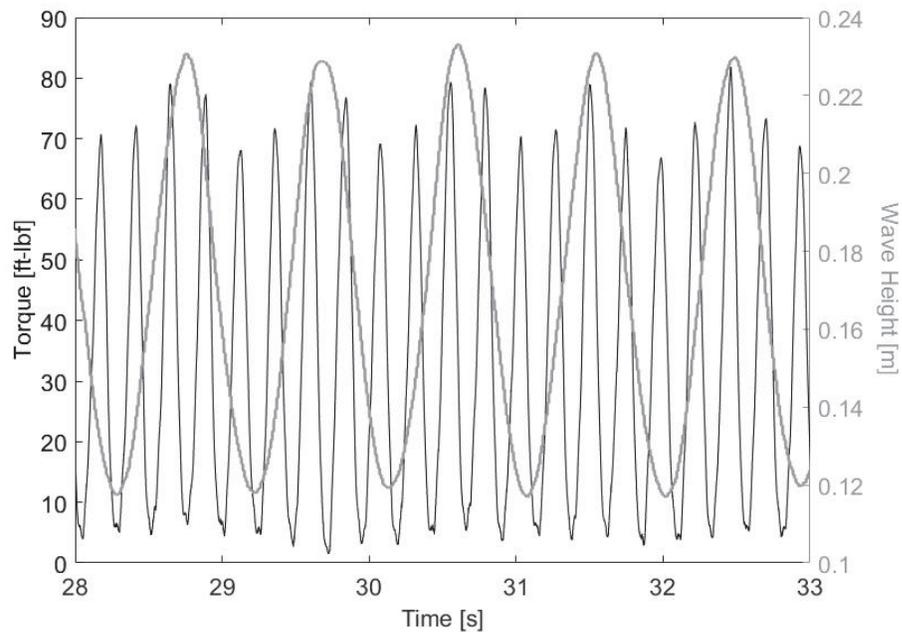**Figure 20:** Turbine torque over time under steady conditions.

Figure 21: Turbine torque over time under 0.1 m, 1.5 sec waves.

The coefficient of power was also plotted for both steady (Figure 22) and unsteady flow conditions (Figure 23) over a single rotation of the turbine. The coefficient of power varies with the turbine torque and shaft speed and demonstrates a similar trend as the turbine torque over a single rotation. Figure 23 illustrates that the incident waves caused more variability in the

coefficient of power due to the similar effect that they had on the turbine torque under the same conditions (Figure 25).
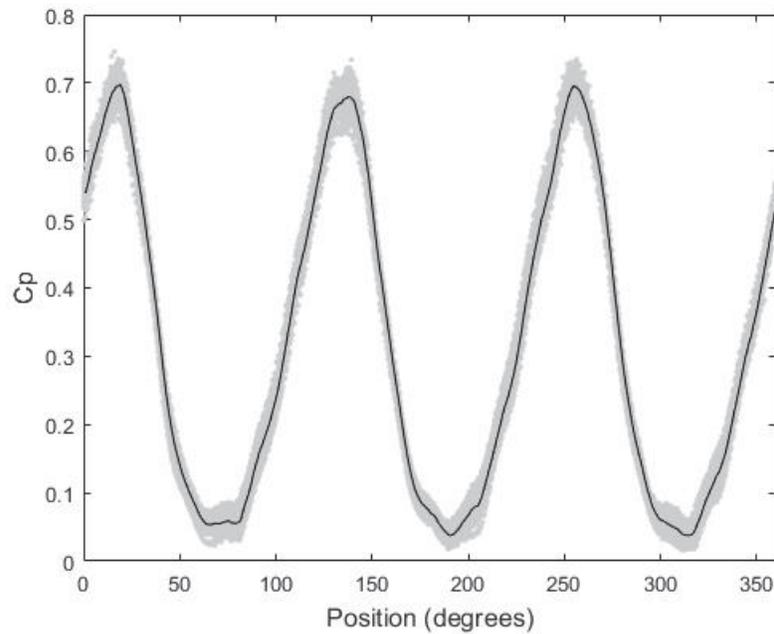

Figure 22: Coefficient of power over one turbine rotation under steady conditions.
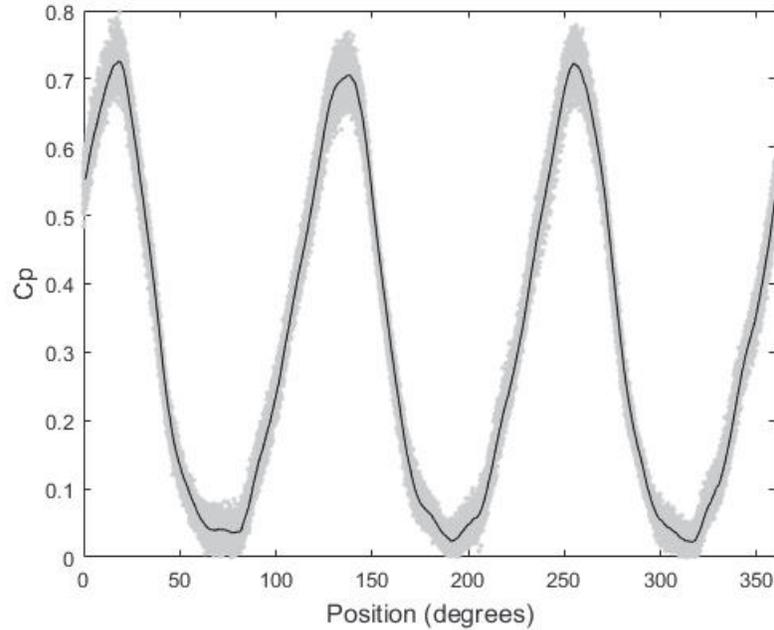

Figure 23: Coefficient of power over one turbine rotation under unsteady conditions.

Performance Characteristics: Comparison of Experimental Results and Theoretical Predictions

The computational model was used to predict the performance of the turbine under both steady (Figure 24) and unsteady flow conditions (Figure 25) over a single rotation of the turbine. Both

figures show that the model captures the correct trend of the measured torque and Figure 25 demonstrates that the model successfully captures the instantaneous effect of the waves on the loading of the turbine blades during rotation. This is evidenced by the variation of peak to trough torque with the inclusion wave velocity. The model does not take into account many of the complex hydrodynamics that affect the power generation of the turbine including tip losses, strut losses and the wake from upstream blades interacting with downstream blades.
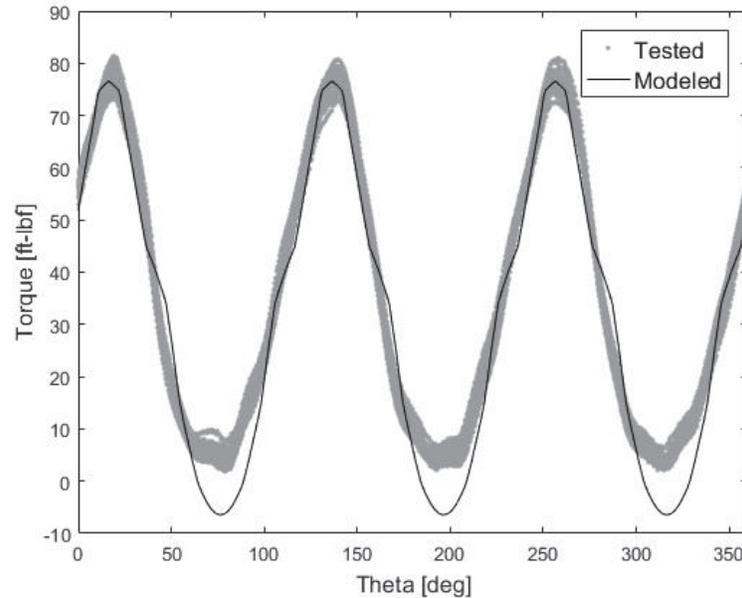

Figure 24: Modeled torque plotted against experimental torque over one turbine rotation under steady conditions.
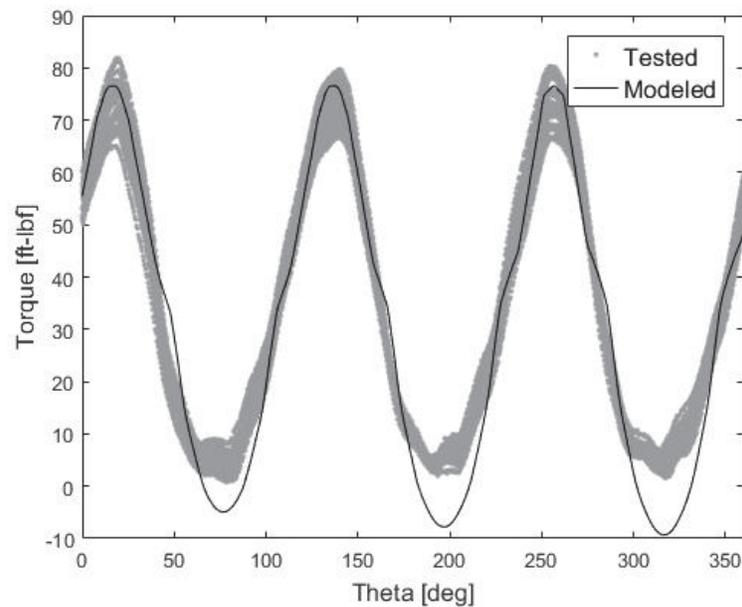

Figure 25: Modeled torque plotted against experimental torque over one turbine rotation under 0.1 m, 1.5 sec waves.

The average experimental turbine performance was compared to the developed computational model at a diameter based Reynolds number of 1.4×10^6 (Figure 26). Due to limitations of the computational model, only the peak performance of the model was predicted to within 10% of its experimental value. As discussed in the methods of analysis section, the computational model is a numerical implementation of an analytical model that utilizes empirical lift and drag data to determine the associated forces on the turbine blades during rotation. This model accounts for the changing velocities of each blade at each point along a rotation to include incident flow velocity, blade rotational velocity, and incident wave velocity.

Though the model was run at the same conditions as the experiments, the angle of attack of the turbine blades in the model never reached a high enough value for the drag force to overcome the lift force and decrease turbine performance beyond the peak. The result is that the model does not capture a degradation in performance experienced by the actual turbine. Specifically, the model does not account for other, more complicated effects such as vortex shedding, wake turbulence, and turbine tip losses which clearly impact performance. Therefore, despite reasonable success in predicting performance for other turbines in other flow regimes, the computational model was determined to be too simple to accurately predict the performance of this model cross flow turbine outside of its peak performance.
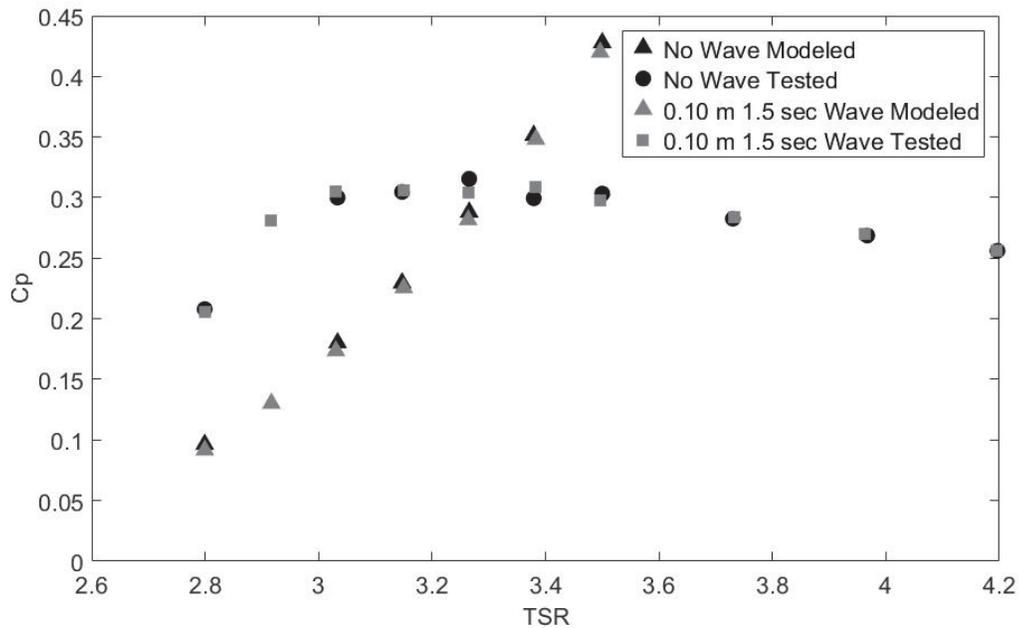

Figure 26: Performance characterization of the model turbine under steady flow conditions compared to the developed computational model.

Conclusions

Experiments were performed on a three-bladed cross flow hydrokinetic turbine in quiescent conditions and in the presence of surface waves, at various Reynolds numbers, and at various blade tip depths. Additionally, a computational model was developed to predict the performance of the turbine in both steady and unsteady flow conditions.

Results indicate that peak turbine performance ($C_p = 0.32$) occurs at a tip speed ratio of about 3.2. Results are lower than previously published performance values due to differences in experimental conditions. The turbine was tested at a range of tow speeds and rotation rates to test scale similarity. Reynolds number independence was not conclusively achieved in these tests, which is necessary for scale independence. Up to a critical depth of approximately half a blade height, turbine operation closer to the free surface slightly increases turbine performance likely due to flow acceleration near the free surface. The turbine was also tested with waves that simulate deep water waves in a riverine environment. While the impact of unsteady flow conditions on the average turbine performance was not significant, unsteady flow conditions have an impact on instantaneous turbine performance, namely blade loading and instantaneous power quality. Lastly, the computational model developed to predict the performance of the turbine was able to capture the correct trends of the torque signal but did not capture certain complex hydrodynamics such as vortex shedding, wake turbulence, and turbine tip losses.

References

[1]   Garrett, Chris, and Patrick Cummins. "Generating power from tidal currents." *Journal of waterway, port, coastal, and ocean engineering* 130.3 (2004): 114-118.

[2]   Energy Information Administration. Annual electricity overview, 2015. http://www.eia.gov/electricity/. Accessed January 2nd, 2016.

[3]   U.S. Department of Energy: Marine and Hydrokinetic Technologies. 2014 Water Power Program Peer Review. Compiled presentations, February 24-28, 2014.

[4]   Khan, M. J., M. T. Iqbal, and J. E. Quaicoe. "Towing tank testing and performance evaluation of a permanent magnet generator based small vertical axis hydrokinetic turbine." *Power Symposium, 2008. NAPS'08. 40th North American*. IEEE, 2008.

[5]   Khan, M. J., et al. "Hydrokinetic energy conversion systems and assessment of horizontal and vertical axis turbines for river and tidal applications: A technology status review." *Applied Energy* 86.10 (2009): 1823-1835.

[6]   Luznik, Luksa, et al. "The effect of surface waves on the performance characteristics of a model tidal turbine." *Renewable Energy* 58 (2013): 108-114.

[7]   U.S. Navy. "Energy." Accessed December 29th, 2015. greenfleet.dodlive.mil/energy

[8]   "Background: Tidal Stream Turbines." www.tidalstream.co.uk. Accessed February 8th, 2016.

[9]   Bryson, George. "Hydrokinetic River Generator Gives Power to Remote Villages in AK." *Northwest Renewable News*. The Anchorage Daily News, 05 Feb. 2009. Web. Accessed 08 Feb. 2016.

[10]   Hill, Craig, et al. "US Department of Energy Reference Model Program RM2: Experimental Results." *Sandia National Laboratories, Albuquerque, NM* (2014).

[11]   Bagbey, R., Jepsen, R., Thresher, R., Copping, A. and Previsic, M. "Marine & Hydrokinetic Reference Model Development." USDE Presentation. 2011.

[12]   Jacobson, Paul T., et al. *Assessment and Mapping of the Riverine Hydrokinetic Resource in the Continental United States*. No. DOE/EE/0002662-1. Electric Power Research Institute, 2012.

[13]   Copping, Andrea E., and Simon H. Geerlofs. "The Contribution of Environmental Siting and Permitting Requirements to the Cost of Energy for Marine and Hydrokinetic Devices." *PNNL-20963* 21 (2011).

[14]   "Darrieus Vertical Axis Turbines," http://www.windturbine-analysis.netfirms.com/index intro.htm

[15]   Islam, M., Ting, D. and Fartaj, A. 2006 "Aerodynamic models for Darrieus-type straight-bladed vertical axis wind turbines," *Renewable and Sustainable Energy Reviews*, 12 1087-1109.

[16]   Faltinsen, O. M. *Sea Loads on Ships and Offshore Structures*. Cambridge: Cambridge University Press, 1999.

[17]   Sheldahl, Robert E., and Paul C. Kilmas. *Aerodynamic Characteristics of Seven Symmetrical Airfoil Sections Through 180-Degree Angle of Attack for Use in Aerodynamic Analysis of Vertical Axis Wind Turbines*. Tech no. SAND80-2114. Albuquerque, NM: Sandia National Laboratories, 1981. Print.

[18]   Lust, Ethan E., et al. "The influence of surface gravity waves on marine current turbine performance." *International Journal of Marine Energy* 3 (2013): 27-40.

[19]   Bachant, Peter, Martin Wosnik, Budi Gunawan, and Vincent S. Neary. "Experimental Study of a Reference Model Vertical-Axis Cross-Flow Turbine." Plos One 11, no. 9 (2016). doi:10.1371/journal.pone.0163799.

[20]   Bahaj, A.s., A.f. Molland, J.r. Chaplin, and W.m.j. Batten. "Power and thrust measurements of marine current turbines under various hydrodynamic flow conditions in a cavitation tunnel and a towing tank." Renewable Energy 32, no. 3 (2007): 407-26. doi:10.1016/j.renene.2006.01.012.

[21]   "HS35 Incremental Optical Encoder." *BEI Sensors*. Web. 29 Nov. 2016.

[22]   McCormick, Michael E. *Ocean Engineering Mechanics: With Applications*. Cambridge: Cambridge UP, 2010. Print.

[23]   "National Data Buoy Center." *US Department of Commerce, National Oceanic and Atmospheric Administration, National Weather Service, National Data Buoy Center*. Web. 29 Nov. 2016.

Appendix A: Uncertainty Analysis

An uncertainty analysis was performed utilizing two runs that were repeated from the baseline no wave tests representing the maximum coefficient of performance. For each run the standard uncertainty was calculated for each of the measured quantities and then propagated to determine the overall uncertainty for each of the calculated quantities. In order to calculate the uncertainty associated with both the torque and the shaft speed, the torque and shaft speed were plotted against the angular position of the rotating turbine (Figure 27 and Figure 28). The average measurement was then calculated for each bin at intervals of 0.1°, which was also plotted against turbine angular position. The Type-A uncertainty associated with both torque and shaft speed was then calculated as the largest difference in measurement within any one bin. Quoted at 95% confidence, the overall uncertainty for the tip speed ratio was quoted at 1.1% and 13% for the power coefficient. This large uncertainty is due primarily to the uncertainty associated with the torque measurement of 11%. Due to the inherent unsteady operation of the turbine itself as well as the considerable model scale the test rig experienced large vibrations that prevented the torque signal from being measured with a higher degree of accuracy.

In the case shown by the Figure 27 and Figure 28, the motor was tasked to maintain 1.35 rotations per second, but the large torque created by the turbine required the motor to periodically compensate. However, by evaluating the oscillating shaft speed with this binning method, the shaft speed was quoted at 95% confidence to an uncertainty of 0.55%.
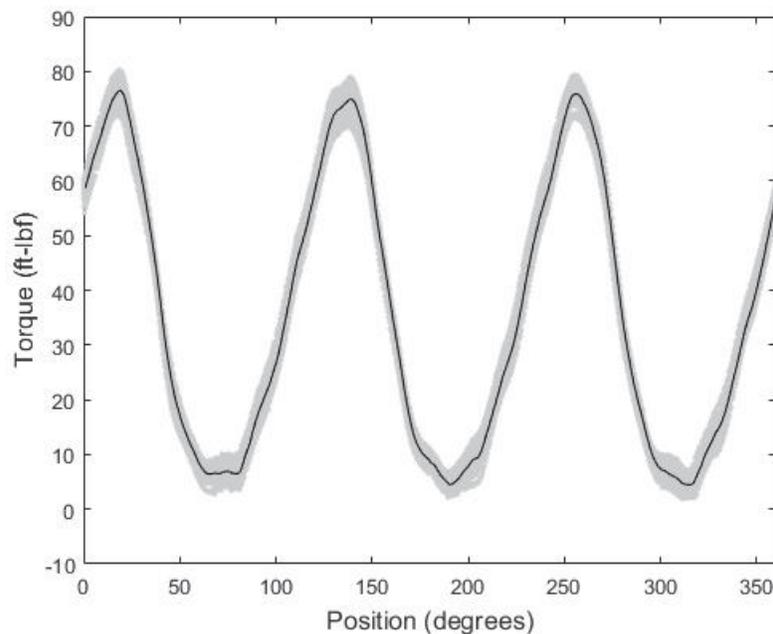

Figure 27: Turbine torque plotted against reference blade position during rotation. This run demonstrates 20 sec of data.
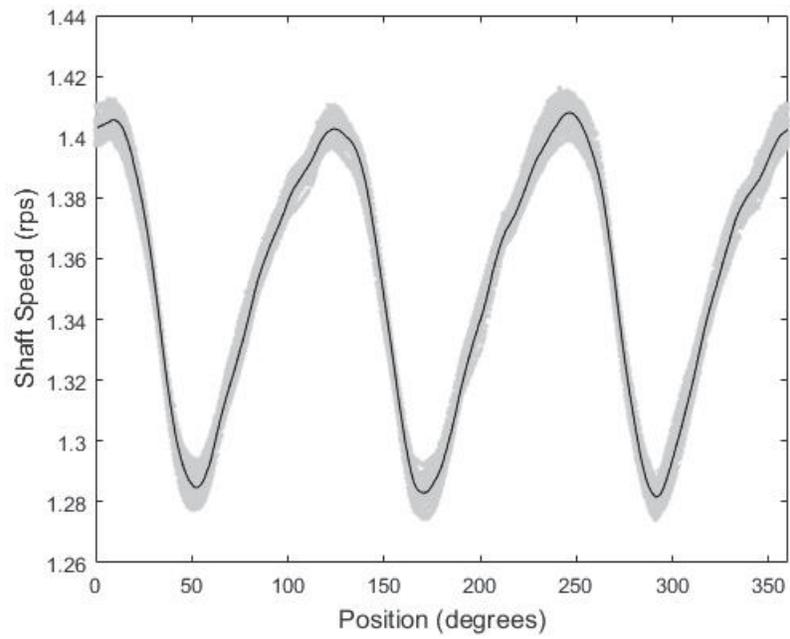
Figure 28: Turbine shaft speed plotted against reference blade position during rotation. This run demonstrates 20 sec of data.